Applied Catalysis B: Environmental 90 (2009) 162–174

Contents lists available at ScienceDirect

Applied Catalysis B: Environmental

journal homepage: www.elsevier.com/locate/apcatb

Development of a Ce–Zr–La modified Pt/γ-Al_2O_3 TWCs' washcoat: Effect of synthesis procedure on catalytic behaviour and thermal durability

A. Papavasiliou [a], A. Tsetsekou [a,*], V. Matsouka [b], M. Konsolakis [b], I.V. Yentekakis [b], N. Boukos [c]

[a] School of Mining Engineering and Metallurgy, National Technical University of Athens, Iroon Polytechniou, Zografou Campus, 15780 Athens, Greece
[b] Laboratory of Physical Chemistry and Chemical Processes, Department of Sciences, Technical University of Crete, 73100 Chania, Crete, Greece
[c] National Centre for Scientific Research "Demokritos", Institute of Material Science, Agia Paraskevi, 15310 Athens, Greece

ARTICLE INFO

Article history:
Received 30 January 2009
Received in revised form 24 February 2009
Accepted 3 March 2009
Available online 14 March 2009

Keywords:
Coprecipitation
Impregnation
Platinum
Alumina washcoat
Ceria–zirconia
Mixed-oxides
TWCs
Thermal aging
Simulated exhaust conditions
Automotive catalysts

ABSTRACT

In this work the effect of different synthesis routes on the thermal stability and catalytic performance of Ce–Zr–La modified Pt/γ-Al_2O_3 three-way converters (TWCs) washcoat is investigated. The production procedures applied were: (i) simultaneous coprecipitation of γ-alumina and ceria-based solid solution from metal nitrates, (ii) sequential coprecipitation of these components and (iii) wet impregnation with different γ-alumina powders (a commercial and a precipitated one). The performance of the as produced catalysts, after loading on cordierite monoliths (TWCs form) was studied under simulated exhaust conditions at the stoichiometric point. Structural, morphological and catalytic properties of the washcoats were examined after calcination at 600 °C for 2 h and thermal aging at 900 °C for 5 h in air. X-ray diffraction (XRD), transmission electron microscopy (TEM), Brunauer–Emmett–Teller physical adsorption (BET) and diffuse reflectance infrared Fourier transform spectroscopy (DRIFTS) were applied for the correlation of the samples' catalytic behaviour with their microstructure and morphological characteristics. Among the preparation routes examined simultaneous coprecipitation leads to the most thermally stable washcoat; it was found to provide higher dispersion of the oxide modifiers in the alumina carrier impeding that way Pt sintering. TWCs prepared by this route also showed the best catalytic performance providing the maximum NO, CO and C_3H_6 conversions and the lowest *light-off* temperatures.

1. Introduction

Three-way catalytic converters (TWCs) have been successfully used for the control and the suppression of automotive emissions by converting basic air pollutants like CO, C_xH_y and NO_x to their inactive products CO_2, N_2 and H_2O. They usually consist of precious metals such as Pt, Pd and Rh dispersed on an alumina support doped with rare earth oxides serving as structure stabilizers and catalytic activity promoters [1–7]. Ceria has been the most frequently used oxide due to its beneficial properties like the ability to enhance the water–gas shift reaction, to improve catalytic activity at the interfacial metal–support sites, to thermally stabilize the alumina support, to promote noble metal dispersion and to exhibit its own catalytic activity especially when it is used in nanoparticles [8–12]. However ceria's most prominent effect is its ability to undergo rapid redox cycles, $2CeO_2 \rightarrow Ce_2O_3 + (1/2)O_2$, thus acting as an oxygen buffer by storing/releasing O_2 due to the Ce^{4+}/Ce^{3+} redox couple. In this way it maintains constant air to fuel ratio around the stoichiometric value, where an optimal simultaneous conversion of CO, hydrocarbons and NOx pollutants is achieved [8–12].

Since nowadays the control of toxic pollutants during cold start period of TWCs has been of high relevance, taking into account that a significant portion of toxic emissions is produced during this period, alternative designs, which deal with a closer arrangement of the TWC with the engine exit are being explored. Higher mean temperature of TWC operation is expected in these designs. As a consequence, operation at elevated temperature demands catalytic materials with enhanced thermal stability.

Ceria's beneficial properties like oxygen storage capacity (OSC) are closely related to its specific surface area and thus attenuated upon thermal treatment. Sintering of ceria facilitates the sintering of the precious metal, leading to thermal deactivation of TWCs [13,14]. Addition of zirconium is considered the most effective way for ceria stabilization. It has been reported that ceria–zirconia solid solution yields an improvement in ceria's oxygen storage capacity (OSC), redox properties, thermal resistance and catalytic activity at low temperatures [11,15–29]. These improved properties originate from the structural defects induced by Zr^{4+} incorporation in ceria

* Corresponding author. Tel.: +30 210 7722213; fax: +30 210 7722119.
E-mail address: athtse@metal.ntua.gr (A. Tsetsekou).

0926-3373/$ – see front matter © 2009 Elsevier B.V. All rights reserved.
doi:10.1016/j.apcatb.2009.03.006

lattice which enhances mobility of bulk oxygen ions [15,17,20,21]. Previous studies [15,21,24,26] have shown that $Ce_{1-x}Zr_xO_2$ solid solutions with an improved redox behaviour and higher values of OSC are those with the highest content of ZrO_2, which are compatible with the cubic symmetry. For the stabilization of the cubic structure even for high Zr content at elevated temperatures many researchers [30–34] have suggested the addition of trivalent cations M^{3+} ($M = La^{3+}$, Y^{3+}, Ga^{3+}) in the oxide mixture CeO_2–ZrO_2. Vidmar et al. [30] found that the trivalent cations favour phase homogeneity of the CeO_2–ZrO_2 solid solution and improve OSC even at low temperatures.

Apart from the appropriate catalytic materials, the production procedure strongly affects TWCs thermal behaviour [27,35,36]. It has been found that full incorporation of Zr into ceria lattice in order to yield a homogenized material leads to optimal redox behaviour and catalytic properties. According to Kozlov et al. [36], the preparation method provides a different degree of interaction between ceria and zirconia resulting in different redox properties upon thermal treatment. Improved redox behaviour was exhibited by the sample prepared with cogelled method whereas samples prepared by impregnation methods presented a lack of homogeneity and thus deteriorated redox properties. Similar conclusions were derived from the work of Hori et al. [27], who found that CeO_2/ZrO_2 solid solution prepared by precipitation exhibit higher OSC than samples prepared by firing mixtures of acetates, upon aging at 1000 °C.

For improving TWCs thermal behaviour an alumina support is often used, providing high dispersion of $Ce_xZr_{1-x-y}La_yO_{2-\delta}$ solid solution and inhibiting its particle growth upon thermal treatment [19,28,36–44]. Again properties of this composite washcoat strongly depend on the synthesis route applied. Until now the most frequently used method was wet impregnation of commercial alumina powder in an aqueous solution of Ce, Zr and La nitrates or oxides [19,38]. An alternative way is the solid solution synthesis by the precipitation method and its conventional mixing with the alumina powder [35,39]. The simultaneous mixing of all the washcoat components on molecular level by a coprecipitation technique is only very recently preferred and investigated. According to Morikawa et al. [43], when coprecipitating Al_2O_3 together with CeO_2–ZrO_2 solid solution high level of oxygen release rate can be achieved even after thermal aging. In agreement with these findings, Adamopoulos et al. [44] suggested two coprecipitation routes for the development of nanosized Al_2O_3-coated $Ce_{1-x}M_xO_{2-\delta}$ (M = Zr or Ca) that yields enhanced OSC. However the above investigations concern catalytic washcoats with high rare earth oxides concentrations (50–80%) and do not provide a direct correlation of the washcoat properties with the catalytic performance.

Purpose of this work is to elucidate the optimal synthesis route for the development of a thermally stable composite catalytic material, consisting of $Ce_{0.4}Zr_{0.5}La_{0.1}O_{1.95}$ solid solution (20 wt.%) dispersed on a γ-alumina carrier (80 wt.%) with low noble metal loading (0.5 wt.% Pt). Therefore samples prepared by three different production procedures (simultaneous coprecipitation, sequential coprecipitation and wet impregnation) were evaluated upon thermal treatment at 600 °C for 2 h and upon aging at 900 °C for 5 h in static air. The microstructural, morphological and pore structural characteristics of the samples were examined and correlated with their catalytic performance, acquired under simulated exhaust conditions at the stoichiometric point.

2. Experimental

2.1. Catalysts preparation

Catalytic powders were prepared by coprecipitation and impregnation with different starting precursor materials. More precisely two coprecipitation methods: simultaneous and sequential; and the impregnation method employing two different γ-alumina powders: one commercial γ-alumina nanopowder (Aldrich-5016A-150 mesh, 5.8 nm) and one produced from precipitation of $Al(NO_3)_3{\cdot}9H_2O$ (Alfa Aesar, 99.5%) were examined. Furthermore simultaneous coprecipitation was studied by using two different precursors of cerium: cerium (III) nitrate and ammonium cerium (IV) nitrate. In each case the final composition of the support was 80 wt.% of γ-alumina and 20 wt.% of $Ce_{0.4}Zr_{0.5}La_{0.1}O_{1.95}$ mixed oxide. For both coprecipitation methods, a procedure already applied for the production of the $Ce_xZr_{1-x}O_2$ mixed oxides is preferred due to its simplicity and effectiveness [23]. The above supporting materials were then loaded with only one precious metal, Pt, at low loading (0.5 wt.%). A classification of the samples by production procedure and cerium/alumina precursors is given in Table 1.

2.1.1. Preparation of supporting materials

2.1.1.1. Coprecipitation methods. Coprecipitation was conducted in five-necked round bottomed split reactor, which was fitted with a glass stirrer and a pH electrode. The precursor materials used were: $Ce(NO_3)_3{\cdot}6H_2O$, $ZrO(NO_3)_2{\cdot}H_2O$, $La(NO_3)_3{\cdot}6H_2O$ and $Al(NO_3)_3{\cdot}9H_2O$ (Alfa Aesar, 99.5%). Solutions of the above metal nitrates were prepared by dissolving appropriate quantity of each solid in 100 mL of distilled water in order to yield the desirable proportion of Ce:Zr:La = 0.4:0.5:0.1. Solutions were mixed and the pH value was raised and kept around 10 by adding NH_4OH (13.4 M) solution as neutralizing agent. The pH of the solution was measured using a HANNA 8417 pH meter combined with a pH electrode. At the end, the content of the reactor was filtered under vacuum. The resulting precipitates were dried at 110 °C for 12 h and calcined at 600 °C for 2 h.

In simultaneous coprecipitation all solutions were mixed together and reaction occurred at once. In this case two different precursor solutions of cerium were separately used: cerium (III) nitrate, $Ce(NO_3)_3{\cdot}6H_2O$ and ammonium cerium (IV) nitrate and $(NH_4)_2Ce(NO_3)_6$ (Alfa Aesar, 99.5%).

Sequential coprecipitation was carried out in two stages. The first stage involved the precipitation of alumina through reaction of $Al(NO_3)_3{\cdot}9H_2O$ solution with NH_4OH which was added dropwise until the pH value was stabilized at 10, whereas the second stage consisted of the insertion of Ce, Zr and La nitrate precursors in the previous solution and again stabilization of the pH value with dropwise addition of NH_4OH. In this way, $Al(OH)_3$, formed in the

Table 1
Classification and coding of the catalysts based on the preparation method used.

Samples	Preparation method	Ce precursor	Al precursor
C_1	Simultaneous coprecipitation	$Ce(NO_3)_3{\cdot}6H_2O$	$Al(NO_3)_3{\cdot}9H_2O$
C_2	Simultaneous coprecipitation	$(NH_4)_2Ce(NO_3)_6$	$Al(NO_3)_3{\cdot}9H_2O$
SC_1	Sequential coprecipitation	$Ce(NO_3)_3{\cdot}6H_2O$	$Al(NO_3)_3{\cdot}9H_2O$
Imp_1	Wet impregnation	$Ce(NO_3)_3{\cdot}6H_2O$	Commercial powder
Imp_2	Wet impregnation	$Ce(NO_3)_3{\cdot}6H_2O$	Powder from precipitation of $Al(NO_3)_3{\cdot}9H_2O$

first stage, acts as seeds for the precipitation of Ce, Zr and La hydroxides.

In order to verify that the proportion of 80 wt.% alumina and 20 wt.% mixed oxides as well as the desirable ratio between the metals Ce:Zr:La were achieved with the coprecipitation methods, ICP measurements were conducted. For this purpose, solutions were assayed by inductively coupled plasma-atomic emission spectroscopy (ICP) using a Leeman Labs. Inc. instrument. After stabilization of the pH value of each solution (at 10) and filtration of the precipitate, 10 mL samples were collected and analyzed. The results confirmed that all the amount of the precursor solutions of the metals Ce, Zr, La and Al were precipitated.

2.1.1.2. Wet impregnation. In wet impregnation two alumina powders were used: commercial γ-alumina nanopowder (Aldrich-5016A-150 mesh, 5.8 nm, 155 m^2/g) and one produced from precipitation of $Al(NO_3)_3{\cdot}9H_2O$ (207 m^2/g) using exactly the same procedure and conditions described in Section 2.1.1.1. In both cases alumina powder was impregnated in an aqueous solution of the Ce, Zr and La nitrates, stirred and heated at 80 °C for 6 h, until the excess of water was removed. The as formed paste of the material was dried and calcined using the same conditions as in coprecipitation method.

2.1.2. Active phase (Pt) addition

For the addition of the active phase (Pt) the supports, in the form of powders, were impregnated in an aqueous solution of $Pt(NH_3)_2(NO_2)_2$ (Aldrich, 3.4 wt.% in dilute ammonium hydroxide) with appropriate concentration so as to yield 0.5 wt.% Pt loading in the final catalytic materials. The resulted suspensions were stirred and heated at 80 °C in order to remove the excess of water. The as formed pastes were then air dried overnight at 110 °C and calcined at 600 °C for 2 h.

2.1.3. Impregnation of cordierite monoliths by the washcoat materials

For the washcoat preparation, stabilized slurries with 15 wt.% solid content were produced. For slurry stabilization, a small amount of ammonium salt of the poly-methacrylic acid (NH4-PMA – commercial name Darvan C, R.T. Vanderbilt Co., Norwalk, CT, USA) was used as dispersant [45,46]. The slurries were ball milled with alumina grinding media for 24 h in order to reduce the size of agglomerates produced during heat treatment. Cylindrical cordierite monoliths with 400 square cells/$in.^2$ (manufactured by Corning, USA) and typical dimensions of 22 mm diameter and 10 mm length, were immersed in the stirring slurry for 1 min and dried at 110 °C for 1 h. The excess of slurry was removed by blowing air through the honeycomb channels. Five sequential impregnations were needed in order to achieve the desirable washcoat loading (20 ± 0.5 wt.% of the total monolith weight) and then the samples were calcined at 600 °C for 2 h. The loading percentage was determined by the difference in weight of the monolith before and after its washcoating. The remaining slurry was dried and calcined at exactly the same conditions as the washcoated monoliths and the resulted powder was used for microstructural, morphological and pore structural characteristics evaluation by XRD, TEM, N_2 adsorption and DRIFTS. These samples (powder and monoliths) were hereafter designated as "fresh".

The aging treatment was performed on calcined samples (powder and monoliths) in a muffle furnace in static air at normal atmospheric pressure for a period of 5 h at 900 °C (samples designated as "aged").

Before acquisition of the catalytic activity measurements, the monolithic samples were heated in flowing He (400 °C/1 h/100 $cm^3\ min^{-1}$), followed by reduction with H_2 (400 °C/1 h/100 $cm^3\ min^{-1}$).

2.2. Catalysts characterization methods

2.2.1. Microstructure and morphology characterization of the catalysts

The following techniques were used for the chemical, microstructure network and morphology analysis of the catalytic samples listed in Table 1.

2.2.1.1. X-ray diffraction (XRD). The X-ray diffraction patterns (XRD) were acquired on a Siemens D5000 diffractometer using nickel-filtered Cu Kα1 radiation (=0.15405 nm), 40 kV voltage and 40 mA current. The following conditions were used: 0.02°/step with integration times of 13 s/step between $2\theta = 15°$ and 85°.

2.2.1.2. N_2 adsorption measurements – BET surface area. The nitrogen adsorption isotherms and BET surface areas were measured at −196 °C with a Quantachrome Nova 1200 equipment. Specific surface area of the catalytic samples was determined by nitrogen physical adsorption using the Brunauer–Emmett–Teller (BET) method. Prior to the measurements the samples were degassed at 250 °C for 2 h under vacuum. The pore size distribution was calculated from the BJH model (Barrett, Joyner and Halenda) using the desorption branch of the isotherm.

2.2.1.3. Transmission electron microscopy (TEM). Transmission electron microscopy (TEM) examinations of dispersed powder specimens were conducted using an FEI CM20 TEM equipped with an EDAX super ultra thin window analyzer for energy dispersion X-ray spectroscopy (EDS) and a Gatan GIF 200 energy filter that was used for elemental mapping. The sample spot for EDS analysis was in the 20–50 nm range. Portions of samples were crushed in an agate mortar and suspended in ethanol. After ultrasonic dispersion, a droplet was deposited on a copper grid supporting a perforated carbon film. Bright field micrographs, selected area electron diffraction (SAED) patterns, high resolution (HREM) images and elemental maps were recorded over selected areas, the composition of which has been measured by EDS.

2.2.1.4. Evaluation of the Pt dispersion by means of IR spectroscopy. In the present study the Pt dispersion was evaluated by a DRIFTS-aided method based on CO chemisorption. Diffuse reflectance IR (DRIFTS) spectra were taken using an Excalibur spectrometer FTS 3000, equipped with an MCT detector cooled by liquid nitrogen and an IR cell (Specac, Environmental Chamber DRIFT model) designed for in situ sample treatment. Spectra were obtained with a resolution of 2 cm^{-1} and accumulation of 64 scans. During these measurements the external optics were purged with CO_2-free dry air generated from an air purifier system (Claind Italy, CO_2-PUR model). Catalytic samples (∼80 mg) in powder form were placed in the IR cell and their surface was carefully flattened in order to maximize the intensity of the IR beam. Before CO adsorption at room temperature, all samples were pretreated as follows: (i) heating to 400 °C under He flow, (ii) reduction with 20% H_2/He at 400 °C for 1 h, (iii) purging with He at 400 °C for 30 min, (iv) cooled to room temperature under He flow and (v) background spectra acquisition under He flow. After this treatment CO was introduced onto the reduced samples (0.5 kPa) and spectra were recorded until steady state (saturation of Pt sites with CO). Then the gas phase was evacuated and an infrared spectrum was collected from which the CO integrated area was estimated.

2.2.2. Catalytic activity measurements

Catalytic activity measurements were carried out in a 300-mm long tubular quartz continuous flow reactor (24 mm i.d.), loaded with the monolithic catalyst (400 cells/$in.^2$ and ∼4 cm^3 volume) in

the middle. A centred K-type thermocouple was used for the measurement of monolithic specimen temperature.

Air Liquide certified gas mixtures, 7.83% NO in He, 10.1% CO in He, 10% C_3H_6 in He and 20.7% O_2, were used. These were further diluted in ultrapure He (99.999%) and supplied to the reactor at 1 bar. Reactant gases were delivered by a series of independent mass flow controllers (MKS type 247). The feed composition during catalytic experiments was 0.1% NO, 0.7% CO, 0.1067% C_3H_6 and 0.78% O_2 balanced with He. The total gas flow rate was 3200 cm^3(STP)/min corresponding to a gas hourly space velocity (GHSV) of 50,500 h^{-1}.

The redox characteristic of the simulated gas mixture was identified by the air–fuel ratio, A/F:

$$\frac{A}{F} = \frac{14.63}{1 + 0.02545\{[CO] + 9[C_3H_6] - 2[O_2] - [NO]\}}$$

or by the stoichiometric number S:

$$S = \frac{2[O_2] + [NO]}{[CO] + 9[C_3H_6]}$$

For the reactants composition applied, the A/F is equal to 14.63, whereas the number S is equal to unit, corresponding to stoichiometric point.

The reactor inlet and outlet were analyzed using an on-line chemiluminescence NOx-analysis (Thermo Environmental Instruments 42C) for NO/NO_2 analysis and an on-line gas chromatography (Shimatzu-14B) for CO, CO_2, O_2, N_2, N_2O and C_3H_6. Before measurements were taken, the catalysts were operated for 1 day under the reactive gas mixture at 500 °C to eliminate possible residue from the metal precursor and to ensure stable operation.

The conversion performance of TWCs specimens was studied by increasing the reactor temperature stepwise from 50 to 550 °C. At each step the temperature was held constant for at least 30 min before catalytic activity measurements.

3. Results

3.1. Microstructure and morphology characterization of the catalysts

3.1.1. XRD analysis results

The XRD patterns of the fresh samples are presented in Fig. 1. The patterns consist of low intensity peaks from two phases: γ-Al_2O_3 and a phase of cubic symmetry with reflections typical of the fluorite structure of CeO_2, corresponding to the (1 1 1), (2 0 0), (2 2 0) and (3 1 1) lattice planes. Peaks of pure lanthana or zirconia could not be detected indicating the incorporation of La and Zr dopant cations into ceria lattice; peaks of crystallized Pt were not detectable either, due to the low Pt-particle size as verified by DRIFTS-aided measurements of Pt dispersion (see Section 3.1.5). Low intensity and broadening of peaks were assigned to the nanostructure of the composite washcoat. As it can be seen, the insertion of Zr into ceria lattice shifted the peaks to larger 2θ in comparison to pure ceria's peaks which are located at $2\theta = 28.6°$, 33.1°, 47.5° and 56.4° (JCPDS 34-0394). This is in accordance with the great difference between the ionic radii of Zr^{4+} (0.84 Å) and Ce^{4+} (0.97 Å). Therefore the incorporation of Zr into ceria lattice will cause a decline of the lattice constant and will shift the peaks to higher 2θ positions. By comparing the patterns of the different samples prepared, it can be easily seen that the shifting of ceria's peaks was not similar. In the case of the samples prepared by coprecipitation the position of Ce (1 1 1) diffraction has been shifted to $2\theta = 28.9°$, 28.92° and 28.95° for C_1, C_2 and SC_1 samples, respectively. Instead, in the case of the samples prepared by the impregnation employing both γ-alumina powders, the shifting was lower and the respective peaks were located at around $2\theta = 28.67°$. This shifting is an indication of the solid solution formation, although XRD patterns obtained could not allow the precise detection of the formation of a single solid solution due to the low intensity and broad peaks. Nevertheless based on the smaller peaks' shifting observed in the patterns of the samples prepared by impregnation, it could be suggested that this method leads to a lesser degree of incorporation of dopant cations into ceria lattice.

The above conclusion is further confirmed by the investigation of the washcoats thermal stability via XRD analysis of the aged samples. In the case of the samples prepared by all the three coprecipitation procedures (Fig. 2A–C) the patterns consist of: γ-Al_2O_3, δ-Al_2O_3, Pt° and a phase of cubic symmetry assigned to the $Ce_{0.4}Zr_{0.5}La_{0.1}O_{1.95}$ solid solution as found in the fresh samples. The absence of tetragonal phase in combination with the symmetrical shape of the solid solution peaks indicate that no phase segregation of the $Ce_{0.4}Zr_{0.5}La_{0.1}O_{1.95}$ solid solution occurred upon thermal treatment. Furthermore, calcination at elevated temperature did not cause severe sharpening of alumina or solid solution peaks

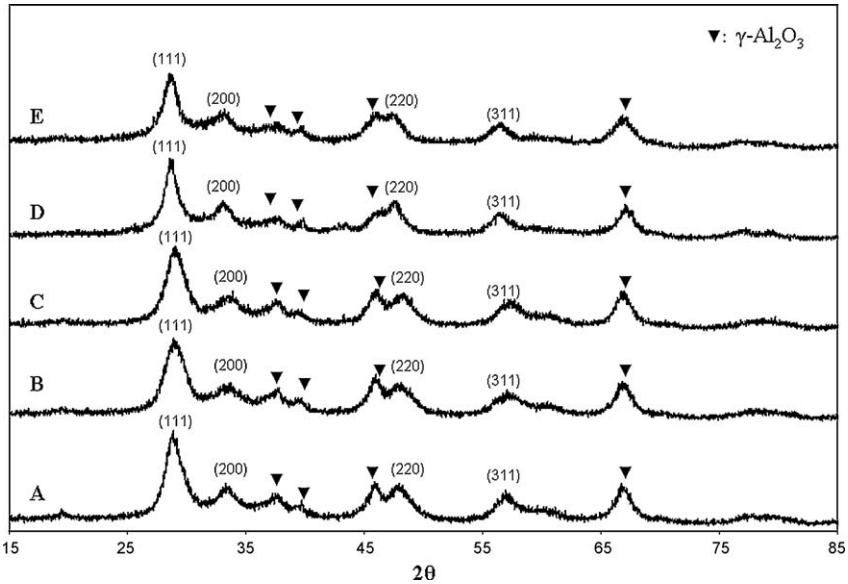

Fig. 1. XRD patterns for the fresh samples: C_1 (A), C_2 (B), SC_1 (C), Imp_1 (D) and Imp_2 (E) as coded in Table 1. The (1 1 1), (2 0 0), (2 2 0) and (3 1 1) ceria lattice planes are indicated; ▼ γ-Al_2O_3.

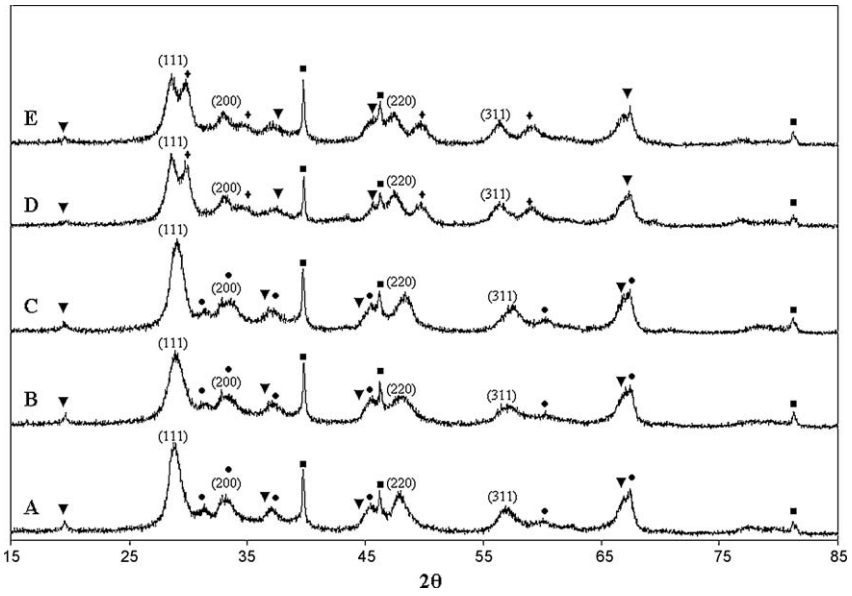

Fig. 2. XRD patterns for the aged samples: C_1 (A), C_2 (B), SC_1 (C), Imp_1 (D) and Imp_2 (E) as coded in Table 1. The (1 1 1), (2 0 0), (2 2 0) and (3 1 1) ceria lattice planes are indicated; (▼) γ-Al_2O_3; (●) δ-Al_2O_3; (■) Pt°; (◆) ZrO_2.

although the phase transformation of γ-Al_2O_3 to δ-Al_2O_3 has already started. In the case of the samples prepared by impregnation (samples Imp_1 and Imp_2 presented in Fig. 2D and E, respectively) peaks of ceria's cubic symmetry, γ-Al_2O_3, Pt° along with ZrO_2 peaks ($2\theta = 29.9°$, $2\theta = 34.8°$, $2\theta = 49.9°$ and $2\theta = 59.5°$) were also detected. This observation confirms that in the latter case Zr dopant was not fully incorporated into ceria lattice at the production stage. In the case of the fresh samples this phase inhomogeneity could not be clearly detected due to the highly dispersed nature of zirconia. However, phase segregation of the solid solution leads to the formation of separate regions of ZrO_2- and CeO_2-rich nanodomains that can further inhibit the contact of alumina particles, thus favouring alumina's thermal stabilization as no transformation was observed in this case. It is worth noticing that in all the catalytic samples examined, thermal treatment at 900 °C revealed all the characteristic peaks of Pt° possibly due to Pt grain growth, as it will be discussed below.

3.1.2. N_2 adsorption measurements – BET surface areas of the samples

The pore structure characteristics (BET surface area, pore volume and average pore diameter) of the fresh and aged catalysts as well as their surface area loss percentage from the fresh state after aging treatment are summarized in Table 2. As it can be observed samples in the fresh state possess high and similar BET surface area (S_{BET}) values. The difference between the two samples prepared by impregnation can be explained by the initial values of S_{BET} of the two alumina powders, which were 155 m^2/g for the commercial alumina (Aldrich) and 207 m^2/g for the laboratory made one. The observed loss of the S_{BET} upon heat treatment at 900 °C was in the range of 41–51% depending on the synthesis route applied with the samples prepared by coprecipitation exhibiting the higher S_{BET} loss.

The nitrogen isotherms at −196 °C for the fresh and aged catalysts are shown in Figs. 3A and 4A, respectively. In the fresh state all the isotherms were of type IV (IUPAC classification) with a hysteresis loop characteristic of mesoporous solids with an open pore system. Figs. 3B and C and 4B and C show the cumulative and differential pore size distributions (PSD) for the fresh and the aged samples, respectively. Fig. 3B and C shows that all the synthesis procedures lead to the formation of materials of similar pore structure presenting a bimodal PSD characterized by a principal peak at 3.5 nm with a shoulder at 5.6 nm and a second peak at around 40 nm. However, in the case of the sample prepared by sequential coprecipitation the volume of pores with sizes at around 40 nm is obviously increased (Fig. 3B and C). This is in accordance with the TEM results, which showed the presence of enlarged alumina grains of about 0.5 μm, as it is discussed below. Upon thermal treatment all samples yield a reduction of the total pore volume and exhibit a shift of the mean pore diameter to higher values. This behaviour is attributed to coagulation of nanoparticles leading to grain growth and thus to elimination of small radii pores and formation of bigger ones. The highest S_{BET} loss and reduction in pore volume is detected in samples C_1 and SC_1 prepared by coprecipitation (Table 3). Observing Fig. 4B and C, it can be derived that the PSD of the sample prepared by impregnation is consisted of a bigger fraction of smaller pores compared to the PSDs of the samples prepared by coprecipitation possibly due to the alumina stabilization by the solid solution segregation (Fig. 4B and C). It is worth noticing that upon calcination at 900 °C all the bimodal PSDs obtained in the fresh samples become narrower.

Table 2
Textural characteristics of the fresh and the aged catalysts prepared by different methods.

Sample	S_{BET} 'fresh' (m^2/g)	S_{BET} 'aged' (m^2/g)	Percentage area loss from the fresh state ΔS_{BET}%	Total pore volume 'fresh' (cm^3/g)	Total pore volume 'aged' (cm^3/g)	Average pore diameter 'fresh' (Å)	Average pore diameter 'aged' (Å)
C_1	195	95	51	0.4	0.33	81	141
C_2	200	111	44.5	0.34	0.33	68	120
SC_1	175	88	50	0.43	0.31	99	140
Imp_1	126	75	41	0.25	0.22	76	115
Imp_2	180	107	41	0.35	0.32	77	121

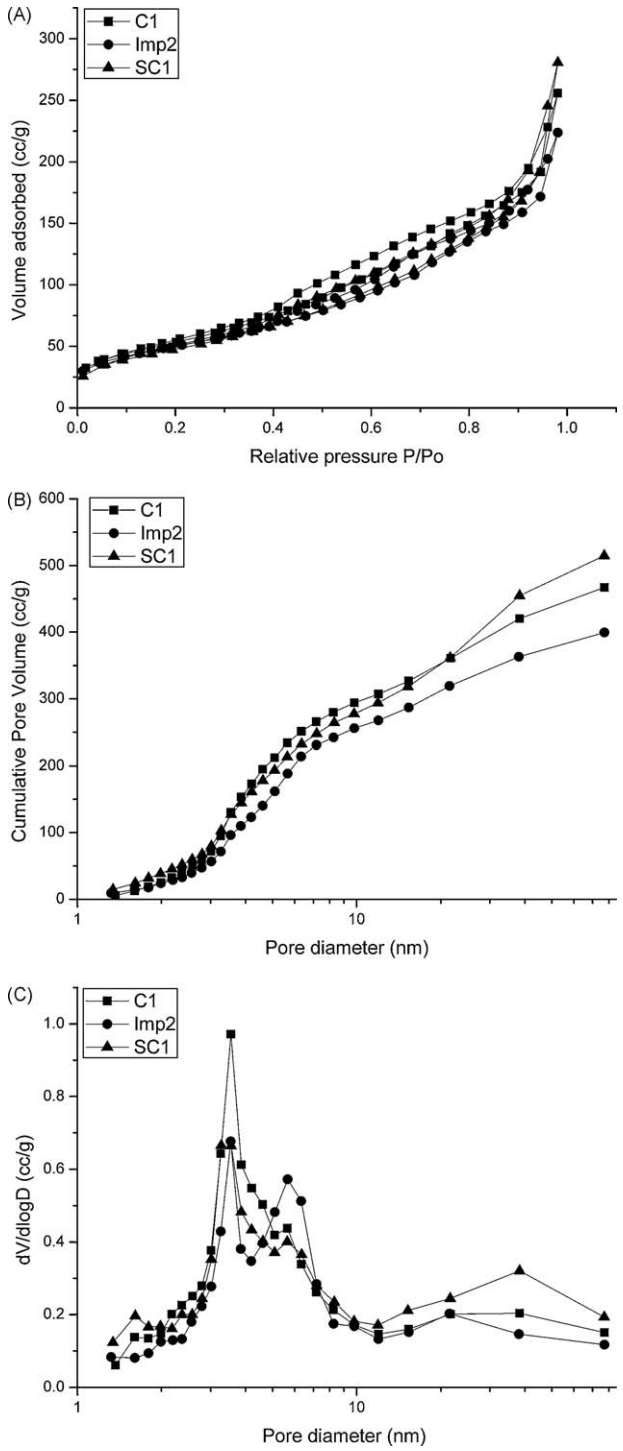

Fig. 3. (A) Adsorption–desorption isotherms, (B) cumulative pore size distribution (CPSD) and (C) differential pore size distribution ($dV - d \log D$) curves for the fresh C_1, Imp_2 and SC_1 samples.

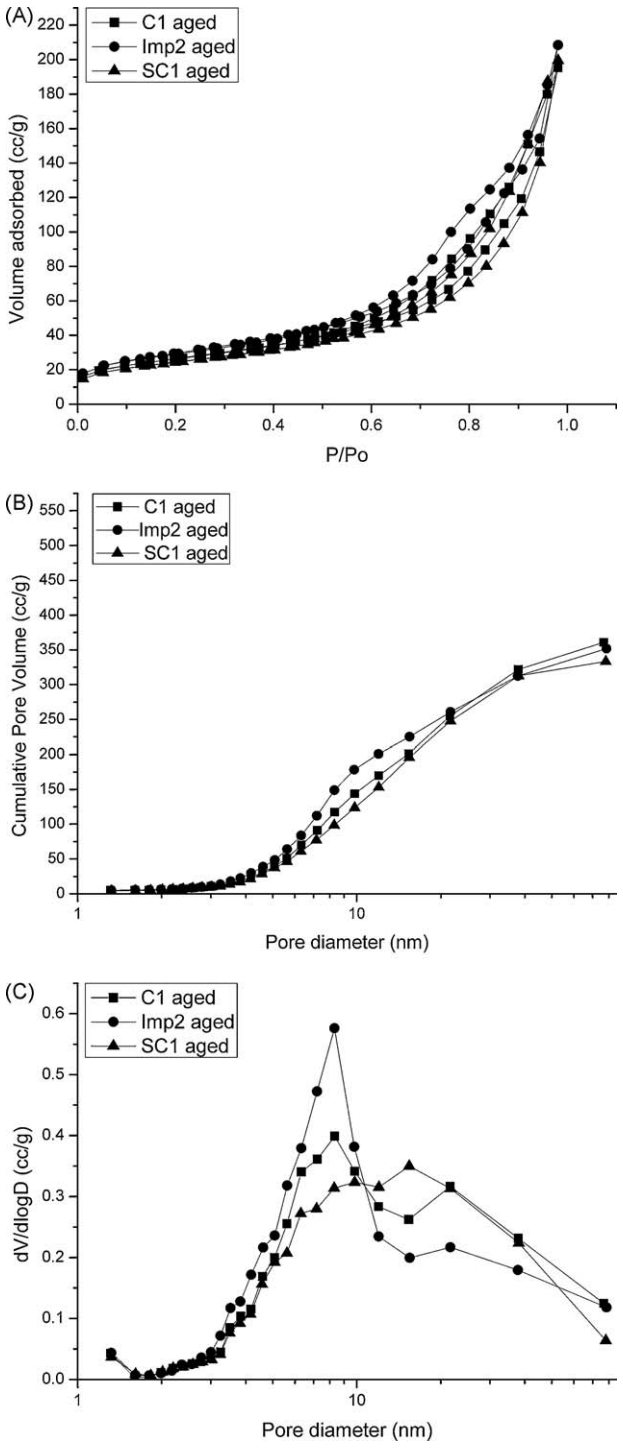

Fig. 4. (A) Adsorption–desorption isotherms, (B) cumulative pore size distribution (CPSD) and (C) differential pore size distribution ($dV - d \log D$) curves for the aged C_1, Imp_2 and SC_1 samples.

3.1.3. TEM characterization of the fresh samples

TEM micrographs of the fresh samples revealed that they consist of two areas: one of alumina and solid solution nanoparticles (Fig. 5A–E) and one of large phylloid formations (Fig. 5F). The images from the coprecipitated samples (Fig. 5A–C) indicate a homogeneous material with sphere-like particles morphology of the order of 2–3 nm. The morphology of the samples prepared by the two impregnation routes is revealed in Fig. 5D and E. The homogeneity of the structure is again apparent, although the particles now possess a more irregular and rod-like shape with diameters of 4–5 nm.

Furthermore, EDS measurements were conducted in the above regions in order to investigate the presence of compositional inhomogeneities in the form of ZrO_2- or CeO_2-rich nanodomains which can generate and accelerate phase segregation of the solid solution at elevated temperatures. For each sample, EDS measurements in 20 different areas were obtained and the average values are reported in Table 3. The standard deviation in all cases did not

Table 3
EDS analysis results for the fresh samples.

Sample	Ce–Zr–La–Al atomic content (%)			
	Ce	Zr	La	Al
C_1	3.2	2.6	1.0	93.2
C_2	1.9	2.4	0.4	95.3
SC_1	10.7	5.3	2.8	81.2
Imp_1	9.0	1.7	1.3	88.0
Imp_2	8.9	1.0	1.0	89.1

exceed 10%. According to Table 3, samples prepared by wet impregnation (catalysts Imp_1 and Imp_2) exhibit much lesser Zr content than the initial Zr loading. On the other hand, in the samples prepared by coprecipitation (catalysts C_1, C_2 and SC_1) the measured Zr content was close to the initial Zr loading, with the sample C_2 presenting the best results. This could indicate that coprecipitation leads to higher degree of incorporation of dopant cations into CeO_2 lattice (as it was also suggested by the XRD patterns of the aged samples) with the highest incorporation being achieved with the use of $(NH_4)_2Ce(NO_3)_6$ as cerium precursor. The latter observation has been also documented in the literature [35] and it is attributed to the structural heterogeneity induced by the difference of precipitation speed of Ce^{3+} and Zr^{4+} ion, because of the great difference of solubility product between $Ce(OH)_3$ (1.5×10^{-20}) and $Zr(OH)_4$ (2×10^{-48}). However, the solubility product of $Ce(OH)_4$ (4×10^{-51}) is closer to that of $Zr(OH)_4$. Another reason, according to Hori et al. [27] and Letichevsky et al. [23], is the presence of cerium (IV) in solution as $Ce(NO_3)_6^{2-}$ anionic complex (unlike cerium (III) that is a hydrolysed cation) which benefits the proximity with the cationic zirconyl (ZrO^{2+}) through an electrostatic mechanism. An additional beneficial factor for the solid solution formation is the fact that tetravalent Ce(IV) exhibits the same valence as Zr dopant.

Phylloid formations observed in the catalytic samples were in the order of 0.1–0.5 μm and are presented in Fig. 5F. Domains of phylloid formations were rarely seen for the samples prepared by simultaneous coprecipitation and were observed in a higher degree in the samples prepared by impregnation methods. More and larger domains were detected in the sample prepared by sequential coprecipitation, which explains the lower SSA values. EDS indicated that these formations are areas of alumina with a small amount of the solid solution. This is also confirmed by SAED patterns (Fig. 5F), in which alumina spots and faint rings indicate the presence of two separate phases. HREM revealed also that the alumina forms very thin single crystalline foils. In Fig. 5F there is a typical HREM image of an alumina particle showing the (1 1 1) lattice fringes.

3.1.4. TEM characterization of the aged samples

The nanostructure nature of the developed washcoats was preserved even after thermal aging as it was revealed by TEM micrographs (Fig. 6). Moreover, phylloid alumina formations in the order of 0.1–0.5 μm, as in the case of the fresh samples, were also detected. TEM micrographs of both the aged samples C_1 and C_2 prepared by simultaneous coprecipitation show a homogeneous material with spherical particles of the order of 5–6 nm (Fig. 6A). In the same regions energy filtered elemental Ce maps demonstrated homogeneous distribution of the solid solution in the alumina carrier (Fig. 6B). Platinum particles could not be visually distinguished from the oxide particles and were detected only by energy dispersion X-ray spectroscopy (EDS) measurements obtained in a larger area.

The catalytic washcoat in the case of both the aged samples Imp_1 and Imp_2 prepared by impregnation is comprised of more elongated particles with diameters of 7–8 nm (Fig. 6C). The analysis showed additionally the presence of some dark areas (Fig. 6E and higher magnification image in the figure insert) which were found by EDS measurements to be distinct ZrO_2 nanodomains dispersed in the alumina washcoat. This is in accordance with EDS investigation on the fresh samples and XRD analysis upon aging which revealed the presence of cerium and zirconium rich nanodomains and ZrO_2 segregation, respectively. Further analysis of the samples by energy filtered elemental Ce maps revealed also a poor dispersion of CeO_2 in the alumina washcoat (Fig. 6D). Additionally, in this case, some enlarged platinum particles (reached in size up to 100 nm), sparsely dispersed in all the area investigated, could be detected (Fig. 6F). It should be mentioned that energy filtered elemental Ce maps revealed that in the areas around the enlarged Pt particles the main phase existing was alumina with negligible amount of ceria-based oxides.

Sequential coprecipitation yields catalytic material consisting of particles with spherical shape and diameters of 6 nm upon thermal aging (Fig. 6G). However, lack of uniformity was revealed in SC_1 sample since islands of solid solution particles in the alumina support were detected and confirmed by energy filtered elemental Ce maps. Large platinum agglomerates up to 100 nm could again be observed as shown in Fig. 6H.

3.1.5. Platinum dispersion

Platinum dispersion on catalytic supports containing ceria-based oxides could not be estimated by commonly used H_2 or CO chemisorption due to the contribution of ceria to the adsorption of both gases [39,47–51]. Additionally, the low contrast between ceria support and Pt particles (similar atomic number) cannot allow the evaluation of Pt dispersion by TEM technique. In our case, a homogeneous Pt distribution cannot be expected due to the composite nature of the washcoat [13] (alumina- and ceria-based oxides). TEM studies have already confirmed the latter by revealing larger Pt particles in alumina-dominated areas. Therefore in the present circumstances TEM analysis can only be used for a general estimation of the extent of Pt grain growth.

In order to pass over the difficulties of measuring Pt dispersion on ceria-containing supported catalysts by conventional CO- or H_2-chemisorption methods, an advanced method was applied in the present work. This method is also based on CO chemisorption, its key difference, however, is the direct measurement of the amount of CO adsorbed on Pt (excluding the CO portion adsorbed on the Ce component of the support) by means of DRIFT spectroscopy. For this purpose, a calibration curve was produced by acquiring the IR spectra of CO adsorbed at room temperature over a series of well characterized 0.5 wt.% Pt/Al_2O_3 catalysts which had been previously imposed to different temperature pretreatments in order to obey a broadened window of Pt-dispersion values; the dispersion of these reference samples, which did not contain ceria, was estimated by the conventional H_2-chemisorption route [53]. The calibration curve is obtained (see Fig. 7a) by measuring the integrated area of the IR peaks that correspond to ν(CO) linearly bonded to *Pt component* of the samples (i.e., CO–Pt, see insert Fig. 7a). Indeed, from the analysis of the ν(CO) region of the IR spectra, different adsorption bands at ca. 2077, 2065 and 1828 cm^{-1} can be assessed (insert Fig. 7a). The first two bands are assigned to CO linearly bonded to surface Pt crystallites; the last one is attributed to doubly bridged Pt_2CO species [50–52]. Since the latter vibration contributes much lesser to the overall adsorption [50–52], the surface Pt atoms can be well approximated by the amount of CO linearly bonded to Pt (which is associated with the integrated area of the corresponding DRIFT spectra peak; insert Fig. 7a). The resulted linear relationship between the integrated area of ν(CO) bands and Pt dispersion (Fig. 7a) can then be employed as a calibration curve for estimating the Pt dispersion

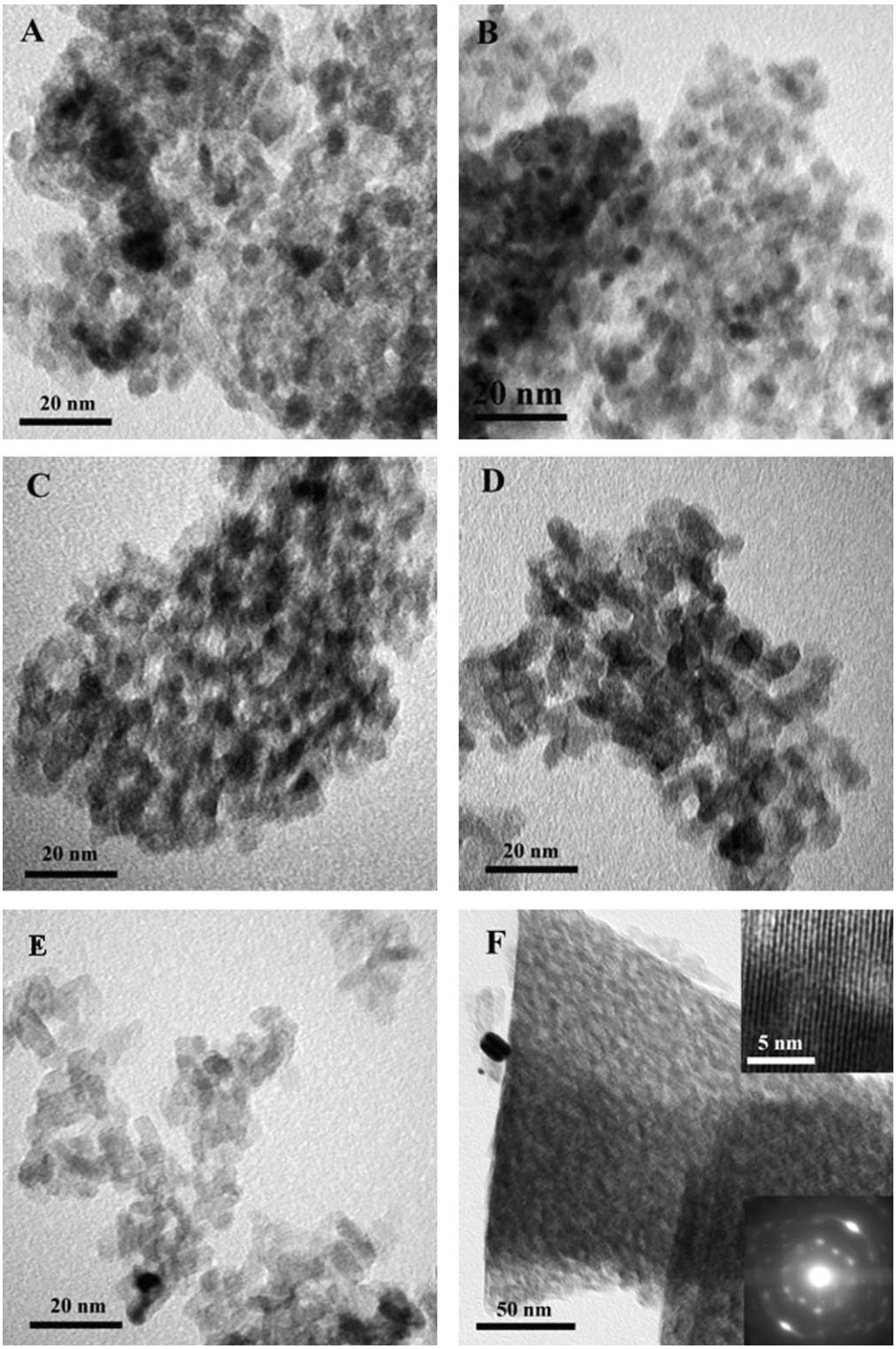

Fig. 5. TEM micrographs of the fresh samples: (A) C_1, (B) C_2, (C) SC_1, (D) Imp_1, (E) Imp_2 and (F) phylloid formation of alumina with SAED pattern and HREM of the alumina area.

on the CeO_2-containing catalysts developed in the present study. For this purpose, the IR spectra of all the catalysts prepared here (Table 1) were acquired at identical conditions (see Fig. 7b), and the respective values of platinum dispersion (Table 4) were estimated as depicted in Fig. 7a.

As it can be observed in Table 4 in the fresh catalytic samples high Pt-dispersion values and accordingly very small crystallite sizes are noticed whereas the different synthesis routes did not modify significantly the results. However after thermal aging a strong reduction of Pt dispersion takes place which amounts about 60% for the samples prepared by coprecipitation and 75–85% for the samples prepared by the other procedures. This has as a consequence the increase of Pt mean size. It becomes obvious that Pt properties upon aging are clearly affected by the synthesis route applied, with the samples by simultaneous coprecipitation presenting Pt-dispersion values more than 100% higher compared

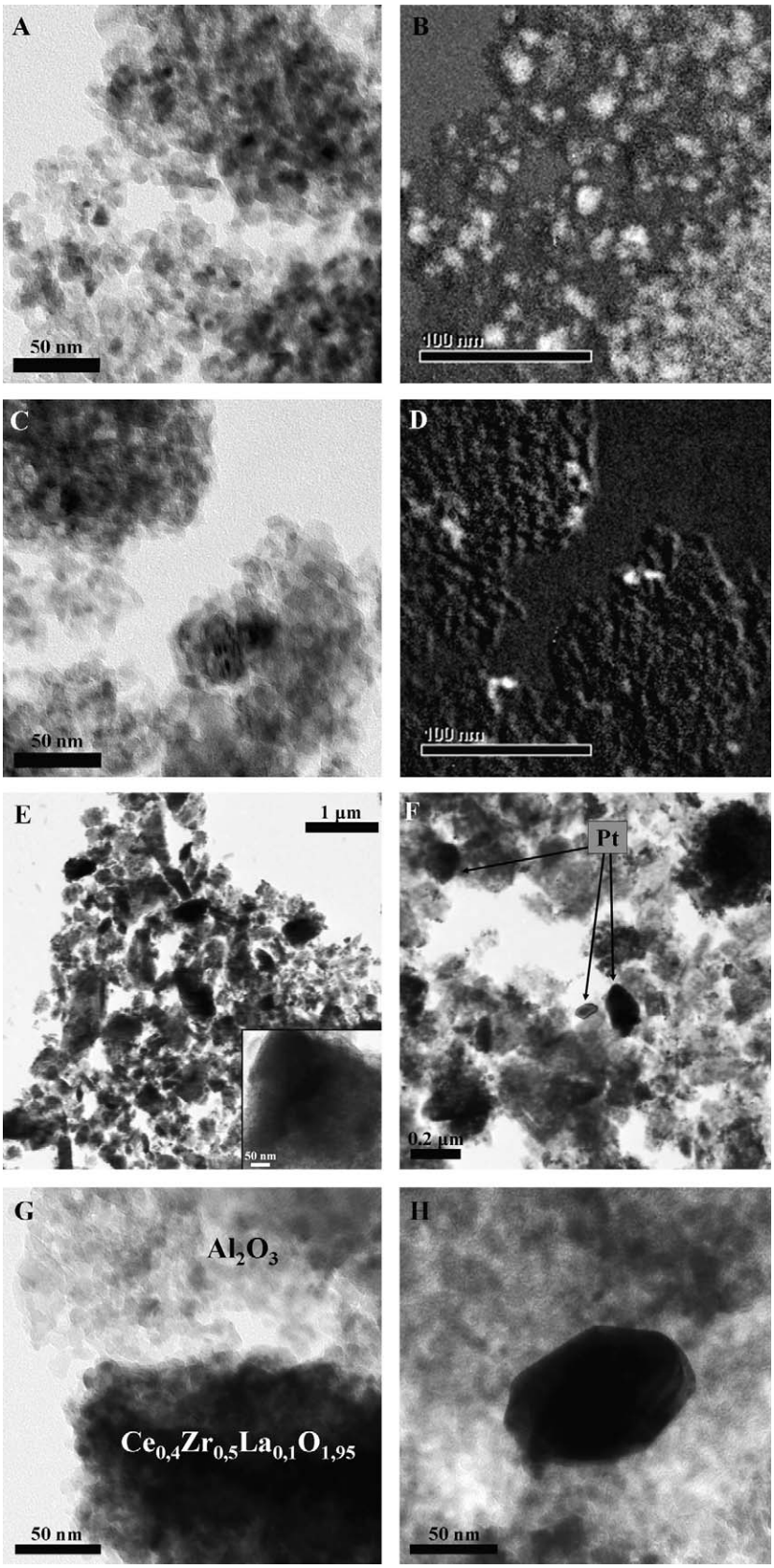

Fig. 6. TEM micrographs of the aged samples: (A) micrograph of C_1 sample with (B) the respective Ce elemental map; (C) micrograph of Imp_2 with (D) the respective Ce elemental map; (E) ZrO_2 nanodomains in the alumina washcoat of Imp_2 sample; (F) enlarged platinum particles detected in Imp_2 sample; (G) micrograph of SC_1 sample; and (H) Pt sintering upon aging in SC_1 sample. The micrographs and Ce maps of C_2 and Imp_1 samples are similar to the images presented for samples C_1 and Imp_2, respectively, and therefore they are not included.

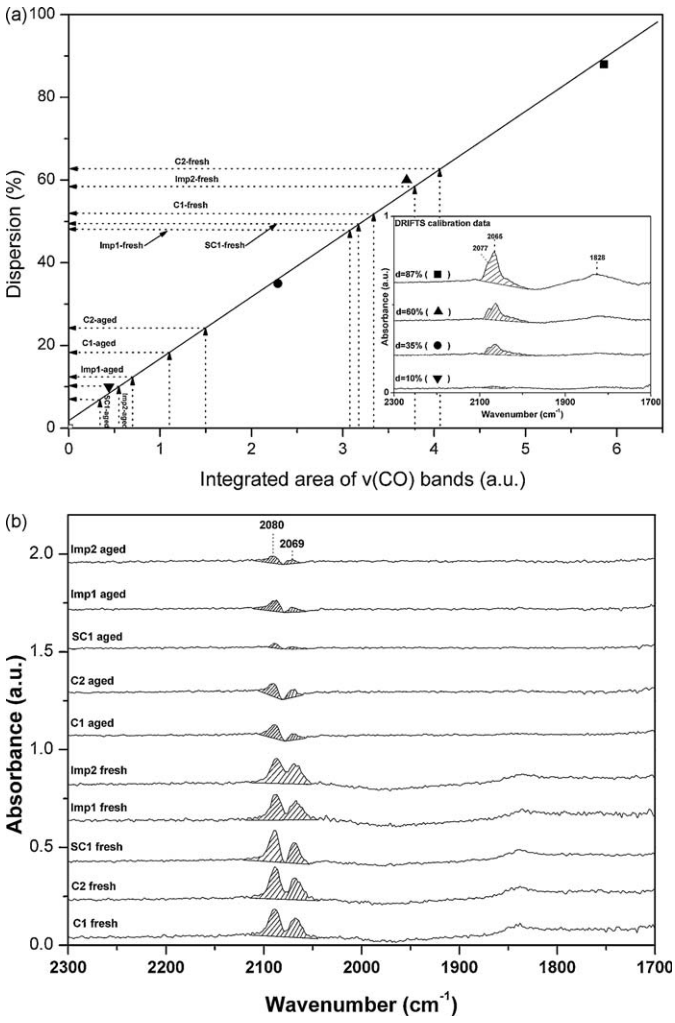

Fig. 7. (a) Calibration diagram for Pt-dispersion evaluation through the integrated area of the ν(CO) peaks of DRIFT spectra associated with the linearly bonded CO with the Pt component of the samples. Insert figure: DRIFT spectra obtained at room temperature after CO adsorption over 0.5 wt.% Pt/Al_2O_3 bare case samples of known dispersions. See text for discussion. (b) DRIFT spectra obtained at room temperature after CO adsorption over the catalytic samples developed (in the fresh and aged state).

to values obtained for the samples prepared by the impregnation or sequential coprecipitation methods.

3.2. Catalyst performance under simulated exhaust conditions – effect of thermal aging on catalysts' performance

The results of three-way catalytic conversion and N_2-selectivity measurements, acquired under simulated exhaust conditions at the stoichiometric point, for the fresh catalysts are presented in Fig. 8. As it can be seen, simultaneous coprecipitation provides the best catalysts (C_1 and C_2) since their *light-off* temperatures, T_{50} (i.e., temperatures for 50% conversion), for all NO, CO and C_3H_6 pollutants are located down to 60 °C lower in comparison to samples prepared by the other methods (Fig. 8a–c). The impregnation method leads to catalysts (Imp_1, Imp_2) with lower conversion activity, whereas the worst behaviour was observed in the catalyst prepared by sequential coprecipitation (SC_1). It is also worth noting that only the catalysts C_1 and C_2 can achieve 100% conversion for all the pollutants in the temperature interval investigated. Similar behaviour was observed for the selectivity towards N_2 (Fig. 8d). The samples prepared by simultaneous coprecipitation (C_1 and C_2) exhibit selectivity values varied at very high levels (87–97%). In contrast, the catalyst synthesized by sequential coprecipitation (SC_1) gives the worst selectivity performance (55–85%). Intermediate selectivity values were observed for the wet impregnated samples (Imp_1 and Imp_2).

The results of the catalytic performance evaluation for the aged samples are plotted in Fig. 9a–d. Among the conversion profiles of the aged catalysts significant differences can be observed. Simultaneous coprecipitation (C_1, C_2) provides catalysts with improved catalytic performance in comparison with the catalysts prepared via impregnation (Imp_1 and Imp_2) or sequential coprecipitation (SC_1). In fact C_1 and C_2 catalysts present the lowest *light-off* temperatures for all the pollutants (~70 °C lower) and the highest conversion values at 500 °C (i.e., ~20–30% higher). Moreover, the selectivity values obtained over these catalysts are ranged at very high levels (80–100%), as in the case of the corresponding fresh catalysts. In contrast, thermal aging markedly affected the samples prepared by wet impregnation (Imp_1 and Imp_2) and sequential coprecipitation (SC_1) as the *light-off* temperatures are very high, varied in the range of 490–540 °C, whereas 50% conversion (especially for NO and C_3H_6) could not be achieved over the whole temperature range investigated (100–550 °C). Finally, catalysts synthesized by wet impregnation (Imp_1 and Imp_2) demonstrate the worst selectivity performance (70–85%), whereas intermediate selectivity values were obtained for sequential coprecipitation (SC_1) prepared samples.

4. Discussion

All synthesis routes yield materials with similar texture – high Pt-dispersion and BET surface area values – and enhanced catalytic behaviour at the fresh state. However thermal aging at 900 °C strongly modifies washcoats physical properties and leads to significant suppression of the catalytic performance of all samples. Loss of the S_{BET} of the produced washcoats facilitates migration and agglomeration of Pt particles, as revealed by the appearance of the characteristic Pt° peaks in the XRD patterns of the aged samples and the reduction of Pt dispersion as indicated by our DRIFTS-aided active surface area measurements. This undesirable Pt grain growth results in attenuating the catalytic performance with the deactivation extent being strongly affected by catalyst's preparation route.

Table 4
Platinum dispersion measured by CO chemisorption followed by IR spectroscopy.

Sample	Fresh			Aged			Percentage dispersion loss (Δd%)
	CO integrated area (a.u.)	Pt dispersion (%)	Mean crystallite size[a] (nm)	CO integrated area (a.u.)	Pt dispersion (%)	Mean crystallite size* (nm)	
C_1	3.34	52	2.7	1.12	19	7.3	63
C_2	4.10	63	2.2	1.50	24	5.8	62
SC_1	3.15	49	2.8	0.33	7	19.7	86
Imp_1	3.11	48	2.9	0.68	12	11.5	75
Imp_2	3.76	58	2.4	0.57	10	13.8	83

[a] Calculations based on Pt surface atom density of 1.53×10^{19} atoms/m^2 [54].

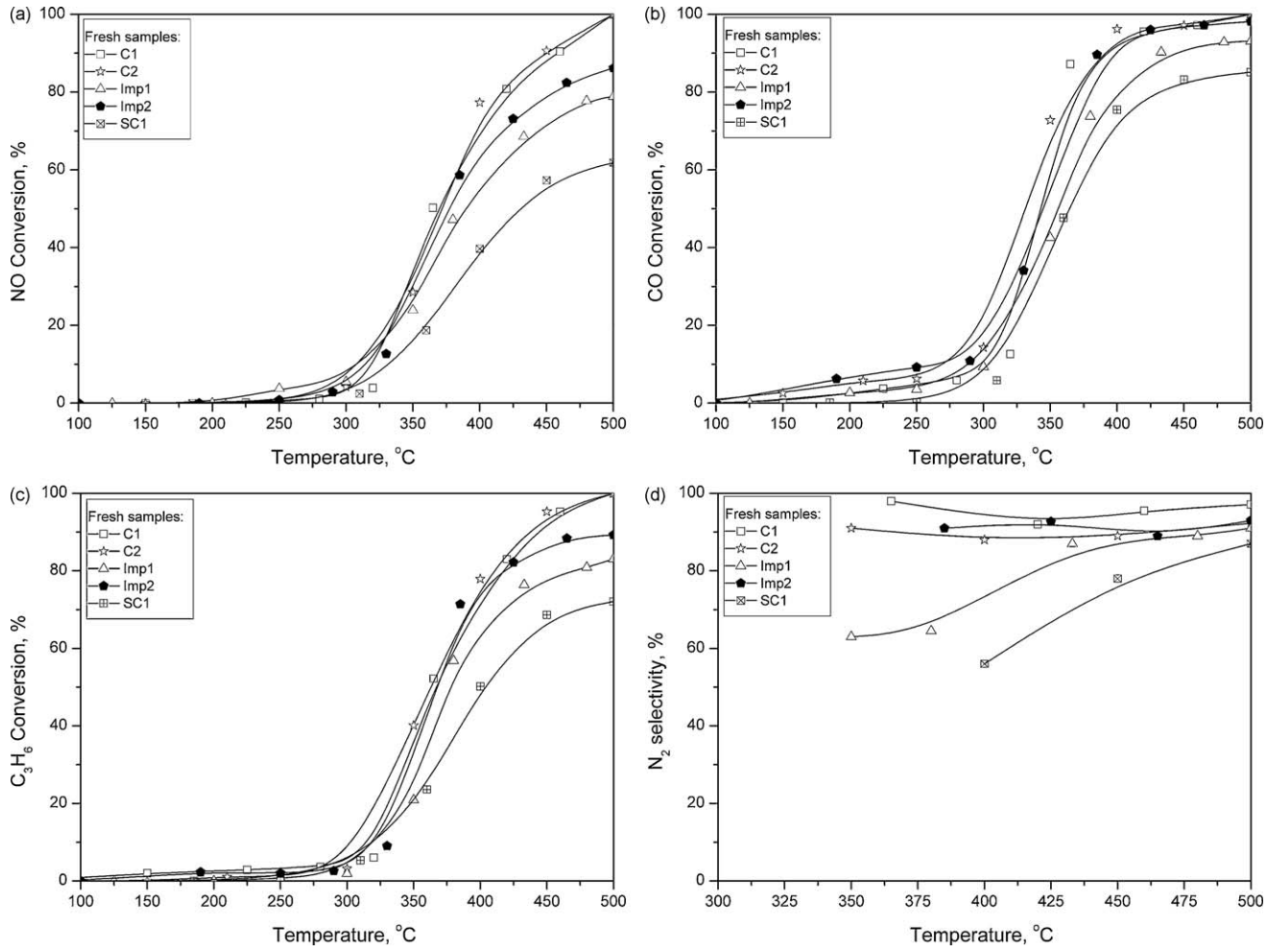

Fig. 8. NO (a), CO (b) and C_3H_6 (c) conversion profiles *vs*. temperature and corresponding N_2-selectivity (d) for the five fresh catalysts listed in Table 1. Conditions: 0.1% NO + 0.7% CO + 0.1067% C_3H_6 + 0.78% O_2 balanced with He at 1 bar. Total flow rate = 3200 cm^3 (STP)/min.

Correlation of textural and catalytic properties of the samples upon thermal aging reveals that the observed differences in S_{BET} values and pore size distribution among the samples cannot account for the observed differences in catalytic activity. For example although the samples C_2 and Imp_2 exhibit similar values of surface area and pore diameter, their catalytic activity differs essentially. Taking into account that all catalysts have the same composition, it can be concluded that the different catalytic performance is attributed to other factors related with the preparation route, such as washcoat homogeneity, Pt dispersion and phase segregation of the solid solution.

Based on the XRD, BET, TEM results and the measured Pt-dispersion values already discussed in combination with the catalytic performances of the prepared samples, it can be concluded that among the synthesis route applied, simultaneous coprecipitation yields washcoats with superior performance in the fresh state and enhanced thermal stability upon aging. More precisely, simultaneous coprecipitation from metal nitrates of all washcoat components allows the preparation of a more homogeneous catalytic material improving significantly the dispersion of the $Ce_{0.4}Zr_{0.5}La_{0.1}O_{1.95}$ solid solution in the alumina washcoat, as demonstrated by TEM analysis. In addition coprecipitation favours the incorporation of dopant cations into ceria lattice and provides the formation of a unique solid solution of the oxide promoters. As a consequence of these structural and morphological properties, better sintering behaviour of washcoat upon aging (preservation of the solid solution dispersion and cubic structure) and lesser grain growth of platinum particles were observed. TEM analysis and Pt-dispersion measurements verified that platinum grain growth was not in great extent, since distinct Pt crystallites could not be visually detected and Pt dispersion was kept in a good level of about 19–24%. Sample C_1, prepared by coprecipitation, presents higher Pt dispersion after aging (the dispersion loss in this case was of the order of 60%) compared with the samples Imp_1 and Imp_2 prepared by impregnation (dispersion loss ~75–85%), although C_1 sample suffers from the highest BET surface area loss among them. These results can be explained based on the previous work of Nagai et al. [13] who studied the sintering inhibition mechanism of Pt in Pt/Al_2O_3 and Pt-/ceria-based oxide catalysts under oxidizing conditions and found that Pt sintering occurs via the molecular migration model [55]. According to their investigation this transport mechanism leading to Pt sintering was inhibited by the strong noble metal–ceria interactions with the formation of Pt–O–Ce bonding which acted as an anchor. Accordingly, in our case, better dispersion of ceria-based oxide on the alumina support (as verified by TEM, Section 3.1.4) enhances prevention of Pt agglomeration. Therefore enhanced homogeneity of the catalytic support and consequently preservation of a good Pt dispersion after aging (Table 4) resulted in a much lesser degree of deactivation with comparatively better conversion values of all pollutants (up to ~25 additional percentage units) and significant differences in *light-off* temperatures (~70 °C lower values) in comparison to samples prepared by the other methods. The key factor for the success of this method is the use of $Al(NO_3)_3{\cdot}9H_2O$

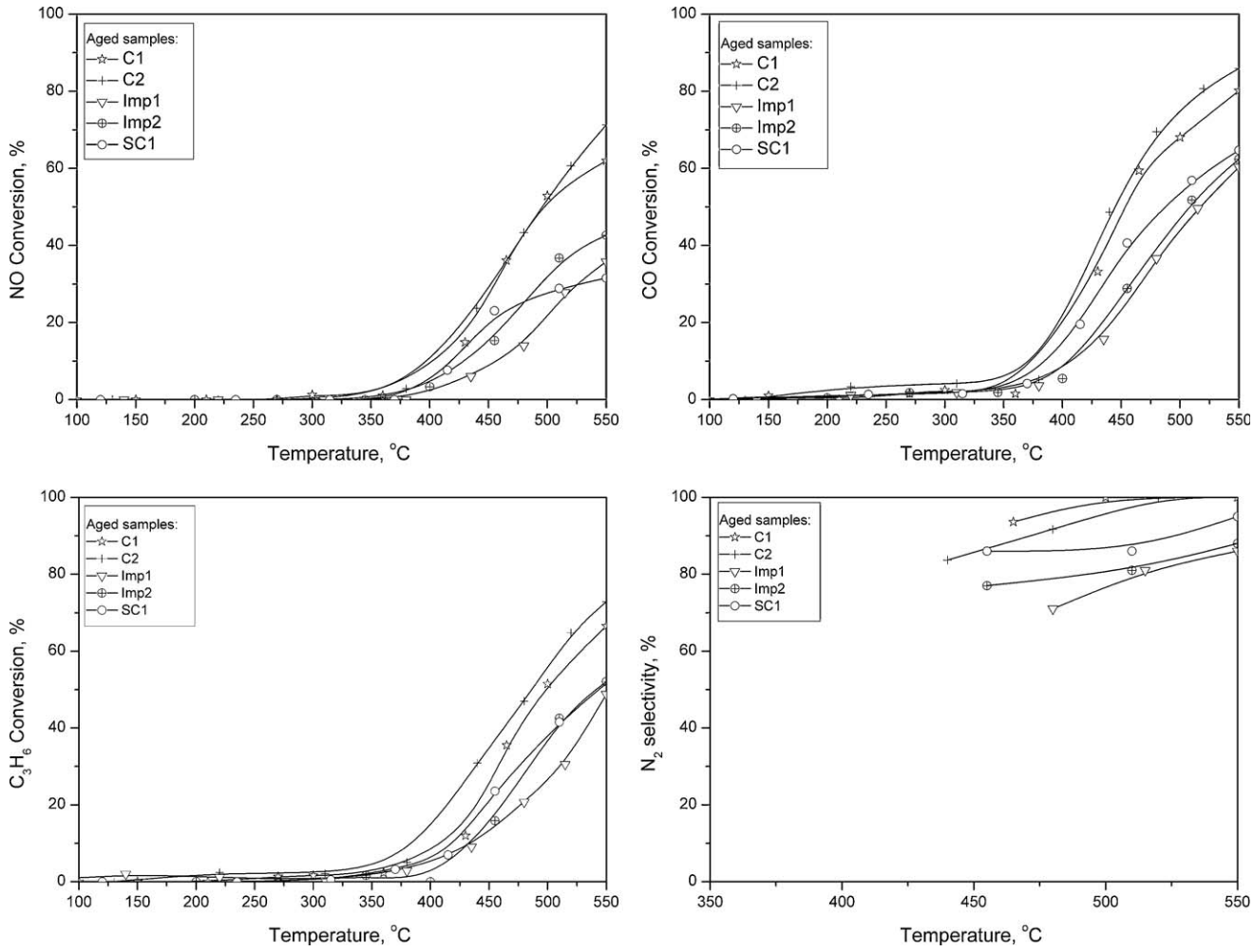

Fig. 9. NO (a), CO (b) and C_3H_6 (c) conversion profiles *vs.* temperature and corresponding N_2-selectivity (d) for the five aged catalysts listed in Table 2. Conditions: 0.1% NO + 0.7% CO + 0.1067% C_3H_6 + 0.78% O_2 balanced with He at 1 bar. Total flow rate = 3200 cm^3 (STP)/min.

instead of alumina powder, allowing better mixing of the components on molecular level.

The fact that different cerium precursor solutions did not have strong impact on the thermal stability and catalytic behaviour is attributed to the presence of the alumina support. As it was revealed by EDS analysis the use of Ce(IV) as a precursor is more effective than Ce(III) regarding the full incorporation of zirconium into ceria lattice. Accordingly, differences in the XRD patterns of C_2 and C_1 samples should be expected with indication of phase segregation in the latter case, as it was documented in previous works [23,27]. Such behaviour is not observed due to the alumina addition which prevents significant particle growth of the metastable $Ce_{0.4}Zr_{0.5}La_{0.1}O_{1.95}$ solid solution (confirmed by TEM investigation) that could lead to the undesirable phase segregation [16,56].

Significantly suppressed catalytic performance was demonstrated by the aged samples prepared by sequential coprecipitation and wet impregnation, with similar conversion values (below 50%) for all the pollutants and high *light-off* temperatures. Major drawback in the sample SC_1 was the lack of uniformity, confirmed by the large amount of alumina domains traced in the fresh sample which were further developed to separate alumina regions and islands of solid solution upon aging (TEM micrographs and energy filtered elemental maps). It is therefore reasonable to suggest that the low catalytic activity at the fresh state is attributed to this uneven distribution of the solid solution which downgrades the Pt–solid solution contacts. The importance of fine dispersion of solid solution particles in an alumina washcoat for achieving increased interfacial metal–support sites and thus enhanced catalytic activity has been also recognized by other researchers [5,43,57,58]. This poor dispersion of the oxide modifiers led upon thermal aging to high surface area loss, coagulation of Pt particles (7% Pt dispersion) and thus to an important degradation of the population of Pt–solid solution interfacial sites which attenuates significantly the catalytic performance.

Samples prepared by impregnation, although they exhibited good catalytic behaviour in the fresh state, upon thermal treatment at 900 °C for 5 h presented severe reduction in conversion values (at around 70%) and in some cases (NO conversion) almost complete deactivation. Suppression of the catalytic performance is again attributed mainly to the poor solid solution and active metal dispersions (10–12%). Large Pt agglomerates with diameters as big as 100 nm were detected by TEM examination confirming considerable Pt sintering. Moreover in this case, phase segregation of the $Ce_{0.4}Zr_{0.5}La_{0.1}O_{1.95}$ solid solution was observed (XRD data and TEM analysis). Phase segregation is strongly undesirable in automotive technology since it results in the formation of two phases, one Ce-rich phase with depressed thermal durability and another Zr-rich phase with poor catalytic activity due to the low reducibility of the tetragonal phase [11,18–21,27,56]. Catalytic activity is closely related to high reducibility of the solid solution and consequently to the preservation of the cubic structure.

However phase segregation of the solid solution upon calcination favoured stabilization of the alumina support by introducing more diffusion barriers, separate regions of ZrO_2- and CeO_2-rich nanodomains, preventing particle to particle contact in the bulk and thus delaying alumina grain growth and transformation [40–43]. This behaviour was revealed by the absence of δ-Al_2O_3 peaks in the XRD patterns and the lowest values of surface area loss obtained by BET measurements.

5. Conclusions

Different synthesis routes (simultaneous coprecipitation, sequential coprecipitation and impregnation) were applied for the development of Ce–Zr–La modified γ-Al_2O_3/Pt washcoat. Catalytic activity measurements under simulated exhaust conditions at the stoichiometric point as well as microstructural and physicochemical studies were conducted to evaluate and compare the catalysts' performance before and after aging treatment at 900 °C.

Among the synthesis routes examined simultaneous coprecipitation yields materials with superior structural, thermal stability and catalytic activity properties. The key factor for this optimum behaviour is the higher degree of washcoat homogeneity which inhibits Pt sintering thus leading to increased noble metal–solid solution interfacial sites.

The study showed that BET surface area is not a significant parameter for catalytic behaviour since samples prepared by impregnation, although they are subjected to the smaller BET surface area loss upon thermal aging, they exhibit the highest degree of deactivation.

Different cerium precursor materials do not have a strong impact both on washcoat structural properties and on catalytic performance upon thermal aging. This result is attributed to the presence of alumina in the washcoat which acts as diffusion barrier inhibiting solid solution grain growth.

Acknowledgements

The authors acknowledge financial support of this work by the PENED 03ED606 research project, implemented within the framework of the "Reinforcement Programme of Human Research Manpower" (PENED) and co-financed by National and Community Funds (75% from E.U.-European Social Fund and 25% from the Greek Ministry of Development-General Secretariat of Research and Technology).

References

[1] J.N. Armor, Appl. Catal. B 1 (1992) 221.
[2] R.J. Farrauto, R.M. Heck, Catal. Today 51 (1999) 351.
[3] J. Kašpar, P. Fornasiero, N. Hickey, Catal. Today 77 (2003) 419.
[4] M. Shelef, G.W. Graham, Catal. Rev. Sci. Eng. 36 (1994) 433.
[5] A. Törncrona, M. Skoglundh, P. Thormählen, E. Fridell, E. Jobson, Appl. Catal. B 14 (1997) 131.
[6] M. Ozawa, J. Alloys Compd. 408–412 (2006) 1090.
[7] M. Ozawa, Y. Nishio, J. Alloys Compd. 374 (2004) 397.
[8] J. Kašpar, P. Fornasiero, M. Graziani, Catal. Today 50 (1999) 285.
[9] S.H. Oh, J. Catal. 124 (1990) 477.
[10] H.C. Yao, Y.F.Y. Yao, J. Catal. 86 (1984) 254.
[11] R.D. Monte, J. Kašpar, Catal. Today 100 (2005) 27.
[12] Z.M. Shi, Y. Liu, W.Y. Yang, K.M. Liang, F. Pan, S.R. Gu, J. Eur. Ceram. Soc. 22 (2002) 1251.
[13] Y. Nagai, T. Hirabayashi, K. Dohmae, N. Takagi, T. Minami, H. Shinjoh, S. Matsumoto, J. Catal. 242 (2006) 103.
[14] S. Suhonen, M. Valden, M. Hietikko, R. Laitinen, A. Savimäki, M. Härkönen, Appl. Catal. A 218 (2001) 151.
[15] G. Vlaic, P. Fornasiero, S. Geremia, J. Kašpar, M. Graziani, J. Catal. 168 (1997) 386.
[16] R.D. Monte, J. Kašpar, J. Mater. Chem. 15 (2005) 633.
[17] E. Aneggi, M. Boaro, C.D. Leitenburg, G. Dolcetti, A. Trovarelli, J. Alloys Compd. 408–412 (2006) 1096.
[18] M. Thammachart, V. Meeyoo, T. Risksomboon, S. Osuwan, Catal. Today 68 (2001) 53.
[19] R.D. Monte, P. Fornasiero, J. Kašpar, P. Rumori, G. Gubitosa, M. Graziani, Appl. Catal. B 24 (2000) 157.
[20] J. Kašpar, P. Fornasiero, G. Balducci, R.D. Monte, N. Hickey, V. Sergo, Inorg. Chim. Acta 349 (2003) 217.
[21] P. Fornasiero, G. Balducci, R.D. Monte, J. Kašpar, V. Sergo, G. Gubitosa, A. Ferrero, M. Graziani, J. Catal. 164 (1996) 173.
[22] M. Ozawa, J. Alloys Compd. 275–277 (1998) 886.
[23] S. Letichevsky, C.A. Tellez, R.R. De Avillez, M.I.P. Da Silva, M.A. Fraga, L.G. Appel, Appl. Catal. B 58 (2005) 203.
[24] Y. Nagai, T. Yamamoto, T. Tanaka, S. Yoshida, T. Nonaka, T. Okamoto, A. Suda, M. Sugiura, Catal. Today 74 (2002) 225.
[25] J.R. González-Velasco, M.A. Gutiérrez-Ortiz, J.-L. Marc, J.A. Botas, M.P. González-Marcos, G. Blanchard, Appl. Catal. B 22 (1999) 167.
[26] P.P. Silva, F.A. Silva, L.S. Portela, L.V. Mattos, F.B. Noronha, C.E. Hori, Catal. Today 107–108 (2005) 734.
[27] C.E. Hori, H. Permana, K.Y.S. Ng, A. Brenner, K. More, K.M. Rahmoeller, D. Belton, Appl. Catal. B 16 (1998) 105.
[28] M. Sugiura, Catal. Surv. Asia 7 (2003) 77.
[29] A.E. Nelson, K.H. Schulz, Appl. Surf. Sci. 210 (2003) 206.
[30] P. Vidmar, P. Fornasiero, J. Kašpar, G. Gubitosa, M. Graziani, J. Catal. 171 (1997) 160.
[31] K. Minami, T. Masui, N. Imanaka, L. Daib, B. Pacaud, J. Alloys Compd. 408–412 (2006) 1132.
[32] L.N. Ikryannikova, A.A. Aksenov, G.L. Markaryan, G.P. Muraveva, B.G. Kostyuk, A.N. Kharlanov, E.V. Lunina, Appl. Catal. A 210 (2001) 225.
[33] H. He, H.X. Dai, L.H. Ng, K.W. Wong, C.T. Au, J. Catal. 206 (2002) 1.
[34] H. Yucai, J. Am. Ceram. Soc. 89 (2006) 2949.
[35] Y. Guo, G. Lu, Z. Zhang, S. Zhang, Y. Qi, Y. Liu, Catal. Today 126 (2007) 296.
[36] A.I. Kozlov, H.K. Do, A. Yezerets, P. Andersen, H.H. Kung, M.C. Kung, J. Catal. 209 (2002) 417.
[37] X. Wu, L. Xu, D. Weng, Appl. Surf. Sci. 221 (2004) 375.
[38] M. Ozawa, K. Matuda, S. Suzuki, J. Alloys Compd. 303–304 (2000) 56.
[39] P.P. Silva, F.A. Silva, H.P. Souza, A.G. Lobo, L.V. Mattos, F. Noronha, C.E. Hori, Catal. Today 101 (2005) 31.
[40] H. Shinjoh, J. Alloys Compd. 408–412 (2006) 1061.
[41] X. Wu, B. Yang, D. Weng, J. Alloys Compd. 376 (2004) 241.
[42] S. Matsumoto, Catal. Today 90 (2004) 183.
[43] A. Morikawa, T. Suzuki, T. Kanazawa, K. Kikuta, A. Suda, H. Shinjo, Appl. Catal. B 78 (2008) 210.
[44] O. Adamopoulos, E. Björkman, Y. Zhang, M. Muhammed, T. Bog, L. Mussmann, E. Lox, J. Eur. Ceram. Soc. 29 (2009) 677.
[45] C. Agrafiotis, A. Tsetsekou, J. Eur. Ceram. Soc. 20 (2000) 815.
[46] C. Agrafiotis, A. Tsetsekou, J. Eur. Ceram. Soc. 20 (2000) 825.
[47] P. Pantu, G.R. Gavalas, Appl. Catal. A 223 (2002) 253.
[48] S. Bernal, J.J. Calvino, M.A. Cauqui, J.M. Gatica, C. Larese, J.A. Perez Omil, J.M. Pintado, Catal. Today 50 (1999) 175.
[49] T. Takeguchi, S. Manabe, R. Kikuchi, K. Eguchi, T. Kanazawa, S. Matsumoto, W. Ueda, Appl. Catal. A 293 (2005) 91.
[50] V. Perrichon, L. Retailleau, P. Bazin, M. Daturi, J.C. Lavalley, Appl. Catal. A 260 (2004) 1.
[51] M. Primet, M.E. Azhar, R. Frety, M. Guenin, Appl. Catal. (1990) 153.
[52] J. Fan, X. Wu, L. Yang, D. Weng, Catal. Today 126 (2007) 303.
[53] M. Konsolakis, I.V. Yentekakis, Appl. Catal. B 29 (2001) 103.
[54] N.M. Markovic, P.N. Ross Jr., Surf. Sci. Rep. 45 (2002) 117.
[55] R.M.J. Fiedorow, S.E. Wanke, J. Catal. 43 (1976) 34–42.
[56] A. Trovarelli (Ed.), Catalysis by Ceria and Related Materials, Catalytic Science Series, vol. 2, Imperial College Press, 2002.
[57] A. Iglesias-Juez, A. Martínez-Arias, M. Fernández-García, J. Catal. 221 (2004) 148.
[58] A. Martínez-Arias, M. Fernández-García, A. Iglesias-Juez, A.B. Hungría, J.A. Anderson, J.C. Conesa, J. Soria, Appl. Catal. B 38 (2002) 151–158.